A New Acceleration Technique With Exponential Convergence Rate to Evaluate Periodic Green Functions

Mário G. Silveirinha, *Member, IEEE,* and Carlos A. Fernandes, *Member, IEEE*

***Abstract*—In this paper we propose a new approach to compute the dynamic potential (Green function) from two- and three-dimensional periodic arrays of point sources in a three-dimensional space. The method has at least exponential convergence rate (in some cases it has Gaussian convergence rate). The convergence rate is independent of the position of the observation point in the unit cell. The proposed approach can also be used to calculate the derivatives of the Green function very efficiently.**

***Index Terms*—Frequency-selective surfaces, homogenization theory, lattice Green function, periodic Green function, photonic crystals.**

I. Introduction

THE solution of Maxwell's equations in periodic unbounded structures can often be reduced to a boundary value problem in a unit cell. An important example is the analysis of doubly periodic systems in a three-dimensional (3-D) space (e.g., frequency-selective surfaces [1]). The Green function method allows formulating the boundary value problem as an integral equation over metallic/dielectric interfaces, and eventually over the boundary of the unit cell.

From the computational point of view, it is desirable that the integral equation domain does not include the boundary of the unit cell since this potentially increases the numerical effort. This can be accomplished by imposing the Green function to satisfy periodic boundary conditions. In that case, the Green function is the dynamic potential from a two-dimensional (2-D) array of point sources in the three-dimensional space. It is sometimes designated as "periodic Green function" [2], but in this paper we shall refer to it as "layer Green function" to avoid confusion with a different Green function introduced ahead. The reason for the designation will be clear later.

It is of crucial importance that the Green function is efficiently evaluated because otherwise the gain obtained in reducing the complexity of the integral equation may be lost in time-consuming computations. Different mathematical representations of the Green function are known. The spatial representation converges always slowly, whereas the spectral representation converges slowly when the observation point lies on the plane of the point sources (the "on-plane" case) [2], [3]. Several methods have been proposed to accelerate the convergence of the corresponding mathematical series. These include the Shanks's transform [4], [5], the summation by parts algorithm [6], and a technique based on the Kummer's transformation and on Poisson's formula [7], [8]. In general, the previous methods have algebraic convergence. In [9] a mixed-domain representation of the Green function is derived (Jordan's formula). This representation has the excellent Gaussian convergence rate, but the important inconvenient of requiring the evaluation of the error function with complex argument, which is computationally demanding. In spite of that, Jordan's formula can greatly reduce the computation time in the analysis of doubly periodic structures [10], [11].

In this paper we propose a new method to efficiently evaluate the "layer Green function" in a 3-D space. The acceleration technique has exponential convergence rate (irrespective to the observation point position), it is valid for arbitrary lattices, and it can also be used to compute the derivatives of the Green function. The idea is that the 2-D array of point sources can be regarded as a sub-lattice of a 3-D lattice. We prove that the potential from the 3-D array of point sources (which we designate as "lattice Green function") is intrinsically related to the layer Green function. We will demonstrate that provided one of the Green functions can be efficiently computed the other one also can. To this end, we will derive new representations for the lattice Green function (one of the representations has Gaussian convergence rate).

The lattice Green function has important applications in many problems. It is used in the Korringa–Kohn–Rostoker (KKR) method to compute the electronic structure of solids in solid-state physics [12]. In [13] the Green function is utilized to calculate the Coulomb interaction energy of a lattice of ions. The lattice Green function plays an important role in the homogenization of artificial materials [14], and in the characterization of the band structure of dielectric and metallic crystals [15]–[17].

The spatial and spectral representations of the lattice Green function converge slowly. In [12] and [18], an alternative spherical wave representation that involves the intensive computation of some lattice constants is presented. In [13], a mixed domain representation with Gaussian convergence rate is derived (Ewald's formula). However, in analogy with Jordan's formula, Ewald's formula requires the evaluation of the error function in the complex plane, which is time-consuming. Indeed, Jordan's formula [9] is intrinsically related to Ewald's original results [13].

Manuscript received April 23, 2003; revised January 17, 2004. This work was supported by the Fundação para Ciência e a Tecnologia under Project POSI 34860/99.

M. G. Silveirinha is with the Electrical Engineering Department, Polo II da Universidade de Coimbra, 3030 Coimbra, Portugal (e-mail: mario.silveirinha@co.it.pt).

C. A. Fernandes is with the Instituto Superior Técnico, Technical University of Lisbon, Portugal (e-mail: carlos.fernandes@lx.it.pt).

Digital Object Identifier 10.1109/TAP.2004.838793

In this paper, we derive three new representations for the lattice Green function: the "spectral-like" representation and two mixed-domain representations. The derived results enable the efficient computation of the lattice Green function and circumvent the shortcomings found in Ewald's formula.

The outline of this paper is as follows. In Section II, we review some standard results concerning the layer Green function. In Section III, we introduce the lattice Green function, and we obtain two new representations for the lattice Green function. In Section IV, we derive a new spectral-like representation for the lattice Green function. The spectral-like representation relates the layer Green function with the lattice Green function. We use this fact to develop a new technique to evaluate the layer Green function. In Section V, we present numerical results that illustrate the efficiency and application of the proposed method, and in Section VI, we draw the conclusions.

II. The Layer Green Function

We consider a 2-D lattice with primitive vectors $\mathbf{a}_1$ and $\mathbf{a}_2$. The primitive vectors define a plane in the 3-D space, which we refer to as the transverse plane. The layer Green function $\Phi_H(\mathbf{r}|\mathbf{r}')$ is the solution of

$$\nabla^2\Phi_H + \beta^2\Phi_H = -\sum_{\bar{I}} \delta(\mathbf{r}-\mathbf{r}'-\mathbf{r}_{\bar{\mathbf{I}}})e^{-j\mathbf{k}.(\mathbf{r}-\mathbf{r}')} \tag{1}$$

where $\mathbf{r}$ is the observation point, $\mathbf{r}'$ is the source point, $\mathbf{r}_{\bar{\mathbf{I}}} = i_1\mathbf{a}_1 + i_2\mathbf{a}_2$ is a generic lattice point, $\bar{\mathbf{I}} = (i_1, i_2)$ is a double-index of integers, and $\mathbf{k}$ is the wave vector that defines the phase shift between the point sources. In addition, the Green function satisfies the usual radiation condition at infinity.

The Green function is the dynamic potential from a 2-D array of phase-shifted point sources positioned at the lattice points $\mathbf{r}' + \mathbf{r}_{\bar{\mathbf{I}}}$. The Green function only depends on the coordinates $\mathbf{u} = \mathbf{r} - \mathbf{r}'$. The spectral representation of the Green function states that [1]

$$\Phi_H(\mathbf{u}) = \frac{1}{A_{\text{cell}}}\sum_{\bar{\mathbf{J}}} \frac{e^{-\gamma_{\bar{\mathbf{J}}}|u_\perp|}}{2\gamma_{\bar{\mathbf{J}}}} e^{-j\mathbf{k}_{\bar{\mathbf{J}},//}.\mathbf{u}} \tag{2a}$$

$$\mathbf{k}_{\bar{\mathbf{J}},//} = \mathbf{k}_{//} + j_1\mathbf{b}_{1//} + j_2\mathbf{b}_{2//};$$

$$\gamma_{\bar{\mathbf{J}}} = \sqrt{|\mathbf{k}_{\bar{\mathbf{J}},//}|^2 - \beta^2} \tag{2b}$$

where $A_{\text{cell}} = |\mathbf{a}_1 \times \mathbf{a}_2|$ is the area of the transverse unit cell, $\bar{\mathbf{J}} = (j_1, j_2)$ is a double-index of integers, $\mathbf{k}_{//}$ is the projection of $\mathbf{k}$ onto the transverse plane, and $u_\perp$ is the projection of $\mathbf{u}$ onto a unit vector normal to the transverse plane. The vectors $\mathbf{b}_{1//}$ and $\mathbf{b}_{2//}$ lie in the transverse plane, and must satisfy $\mathbf{a}_m.\mathbf{b}_{n//} = 2\pi\delta_{m,n}$ for $m, n = 1, 2$, where $\delta_{m,n}$ is Kronecker symbol.

The spectral representation of the Green function converges exponentially except when $u_\perp = 0$, i.e., when the observation point lies "on the source plane." In that important case, the spectral representation converges extremely slowly [7]. This may affect considerably the efficiency of electromagnetic solvers.

III. The Lattice Green Function

In this section we introduce a Green function that is pseudoperiodic in three independent directions of space, in contrast with the layer Green function, which is pseudoperiodic only in two directions.

The Green function is the dynamic potential from a phase-shifted array of point sources positioned at the lattice points of a 3-D lattice. The primitive vectors of the 3-D lattice are $\mathbf{a}_1$, $\mathbf{a}_2$ and $\mathbf{a}_3$. The lattice points are $\mathbf{r}_{\mathbf{I}} = i_1\mathbf{a}_1 + i_2\mathbf{a}_2 + i_3\mathbf{a}_3$, where $\mathbf{I} = (i_1, i_2, i_3)$ is a generic triple-index of integers. We shall refer to the Green function as the "lattice Green function." It is the Floquet wave solution of the following equation:

$$\nabla^2\Phi_p + \beta^2\Phi_p = -\sum_{\mathbf{I}} \delta(\mathbf{r}-\mathbf{r}'-\mathbf{r}_{\mathbf{I}})e^{-j\mathbf{k}.(\mathbf{r}-\mathbf{r}')} \tag{3}$$

where $\mathbf{r}$ is the observation direction, $\mathbf{r}'$ is the source point, β is the wave number, and $\mathbf{k}$ is the wave vector that defines the phase shift between the point sources. The Green function is the dynamic potential from the point sources placed at $\mathbf{r}' + \mathbf{r}_{\mathbf{I}}$. In Section III, we prove that the lattice Green function is intrinsically related to the layer Green function, and we exploit that fact to accelerate the convergence of the layer Green function.

The spatial representation of the lattice Green function is [12]

$$\Phi_p(\mathbf{u}) = \sum_{\mathbf{I}} \Phi_0(\mathbf{u}-\mathbf{r}_{\mathbf{I}})e^{-j\mathbf{k}.\mathbf{r}_{\mathbf{I}}} \tag{4}$$

where $\mathbf{u} = \mathbf{r} - \mathbf{r}'$, and $\Phi_0(\mathbf{r}) = \exp(-j\beta|\mathbf{r}|)/4\pi|\mathbf{r}|$ is the free-space Green function.

By expanding Φ_p and the series in the right-hand side of (3) into plane waves, we obtain a spectral representation for the Green function [12]

$$\Phi_p(\mathbf{u}) = \frac{1}{V_{\text{cell}}}\sum_{\mathbf{J}} \frac{e^{-j\mathbf{k}_{\mathbf{J}}.\mathbf{u}}}{|\mathbf{k}_{\mathbf{J}}|^2 - \beta^2} \tag{5a}$$

$$\mathbf{k}_{\mathbf{J}} = \mathbf{k} + j_1\mathbf{b}_1 + j_2\mathbf{b}_2 + j_3\mathbf{b}_3 \tag{5b}$$

where $V_{\text{cell}} = |\mathbf{a}_1.\mathbf{a}_2 \times \mathbf{a}_3|$ is the volume of the unit cell, $\mathbf{J} = (j_1, j_2, j_3)$ is a triple-index of integers, and $\mathbf{b}_1$, $\mathbf{b}_2$, and $\mathbf{b}_3$ are the reciprocal lattice primitive vectors defined by $\mathbf{a}_n.\mathbf{b}_m = 2\pi\delta_{n,m}$, $m, n = 1, 2, 3$ [12].

Both the spatial and the spectral representations converge slowly, and thus are of limited interest in the numerical evaluation of the lattice Green function. In what follows we derive two new mixed-domain representations for the Green function with excellent convergence rate. The representations are related to Ewald's mixed-domain formula [13]. However, as we shall verify ahead, the new formulas are much more effective from the numerical point of view. Later, we shall prove that the results can be used to accelerate the convergence of the layer Green function.

To begin with, we note that the radiating solution Φ_0 of the Helmholtz's equation in (4) can be replaced by an arbitrary (bounded) solution not necessarily satisfying Sommerfeld's radiation condition. Indeed, the lattice Green function is not required to satisfy any particular radiation condition at infinity because it is a Floquet wave with wave vector $\mathbf{k}$. In particular, assuming that the wave number β is real, we can replace Φ_0 by

$$\Phi_{0,\pm}(\mathbf{r}) = \frac{\cos(\beta|\mathbf{r}|)}{4\pi|\mathbf{r}|}. \tag{6}$$

The function $\Phi_{0,\pm}$ does not satisfy the Sommerfeld's radiation condition. From the previous discussion, we have that

$$\begin{aligned}\Phi_p(\mathbf{u}) &= \sum_{\mathbf{I}} \Phi_{0,\pm}(\mathbf{u}-\mathbf{r_I}) e^{-j\mathbf{k}.\mathbf{r_I}} \\ &= \sum_{\mathbf{I}} \frac{1}{4\pi} \frac{\cos(\beta\rho_I)}{\rho_I} e^{-j\mathbf{k}.\mathbf{r_I}} \\ \rho_{\mathbf{I}} &= |\mathbf{u}-\mathbf{r_I}|. \end{aligned} \tag{7}$$

The equivalence between the previous formula and (4) is the key identity that will allow us to generalize Ewald's results.

The spatial sum (7) converges very slowly. The idea to accelerate the convergence is to use the Poisson summation formula [19]. The Poisson formula transforms a sum in the spatial domain into a sum in the spectral domain, and may dramatically increase the convergence rate of a generic series. Indeed, when a function decays slowly in the spatial domain, it decays in general extremely fast in the spectral domain. However, in this case, the singularity of $\Phi_{0,\pm}$ at the origin prevents its three-dimensional Fourier transform to decay fast at infinity.

To circumvent this situation we consider the decomposition

$$\begin{aligned}\Phi_{0,\pm}(\mathbf{u}) &= \frac{\cos(\beta\rho)}{4\pi\rho} g(\rho) + \frac{\cos(\beta\rho)}{4\pi\rho}(1-g(\rho)) \\ &= f_1(\rho) + f_2(\rho) \end{aligned} \tag{8}$$

where $\rho = |\mathbf{u}|$, f_1 and f_2 are, respectively, the first and second terms of the intermediate identity, and function g is chosen as described in the next paragraphs.

First, we require g to be such that it can be evaluated in an efficient way. Second, we impose that as ρ approaches infinity, g converges exponentially to unity. This ensures that when we substitute (8) in (7), the sum corresponding to the second term converges fast.

The objective is to use the Poisson summation formula to accelerate the convergence of the series associated with the first term. To this end, we require that the three-dimensional Fourier transform of f_1 is known in closed-form. Furthermore, in order to guarantee that the Fourier transform decays fast at infinity f_1 must be a smooth function of $\mathbf{u}$ at the origin. This is possible only if f_1 is an even function of ρ, and thus if g is an odd function of ρ.

Thus, g must be an odd function that converges exponentially to unity as ρ approaches infinity, and such that f_1 is analytically Fourier transformable. In that case, using Poisson summation formula [19], we obtain from (7) and (8) that

$$\Phi_p(\mathbf{u}) = \Phi_{p,1}(\mathbf{u}) + \Phi_{p,2}(\mathbf{u}) \tag{9a}$$

$$\begin{aligned}\Phi_{p,1}(\mathbf{u}) &= \sum_{\mathbf{I}} f_1(\rho_{\mathbf{I}}) e^{-j\mathbf{k}.\mathbf{r_I}} \\ &= \frac{1}{V_{\text{cell}}} \sum_{\mathbf{J}} \tilde{f}_1(-\mathbf{k_J}) e^{-j\mathbf{u}.\mathbf{k_J}} \end{aligned} \tag{9b}$$

$$\begin{aligned}\Phi_{p,2}(\mathbf{u}) &= \sum_{\mathbf{I}} f_2(\rho_{\mathbf{I}}) e^{-j\mathbf{k}.\mathbf{r_I}} \\ &= \sum_{\mathbf{I}} \frac{1}{4\pi} \frac{\cos(\beta\rho_{\mathbf{I}})}{\rho_{\mathbf{I}}} (1-g(\rho_{\mathbf{I}})) e^{-j\mathbf{k}.\mathbf{r_I}} \end{aligned} \tag{9c}$$

where $\mathbf{k_J} = \mathbf{k} + j_1\mathbf{b}_1 + j_2\mathbf{b}_2 + j_3\mathbf{b}_3$, $\mathbf{J} = (j_1, j_2, j_3)$ is a generic triple-index, $V_{\text{cell}} = |\mathbf{a}_1.\mathbf{a}_2 \times \mathbf{a}_3|$ is the volume of the unit cell, and $\tilde{f}_1$ is the Fourier transform of f_1 given by

$$\tilde{f}_1(\mathbf{k}') = \int\int\int f_1(\mathbf{u}) e^{-j\mathbf{k}'.\mathbf{u}} d^3\mathbf{u} \tag{10}$$

where $\mathbf{k}'$ is the Fourier space vector. Equation (9) is a mixed-domain representation of the lattice Green function. The term $\Phi_{p,1}$ resembles the spectral representation of the Green function, whereas the term $\Phi_{p,2}$ resembles the spatial representation.

Since f_1 only depends on $\rho = |\mathbf{u}|$, the triple integral (10) can be reduced to an integral over the real axis. To this end, we consider a spherical coordinate system (ρ, θ, φ) with the polar axis parallel to $\mathbf{k}'$. In this way, we obtain that

$$\begin{aligned}\tilde{f}_1(\mathbf{k}') &= \int_0^\infty \int_0^{2\pi} \int_0^\pi f_1(\rho) e^{-j|\mathbf{k}'|\rho\cos\theta} \rho^2 \sin\theta d\theta d\varphi d\rho \\ &= \frac{4\pi}{|\mathbf{k}'|} \int_0^\infty f_1(\rho)\rho \sin(|\mathbf{k}'|\rho) d\rho \\ &= \frac{1}{|\mathbf{k}'|} \int_0^\infty \cos(\beta\rho) g(\rho) \sin(|\mathbf{k}'|\rho) d\rho. \end{aligned} \tag{11}$$

Similarly the Fourier transform of f_2 is

$$\tilde{f}_2(\mathbf{k}') = \frac{1}{|\mathbf{k}'|} \int_0^\infty \cos(\beta\rho)(1-g(\rho)) \sin(|\mathbf{k}'|\rho) d\rho. \tag{12}$$

In Sections III-A and III-B, we propose specific choices for the g function, and we derive the corresponding mixed representations for the lattice Green function. Our choices are logic, because there are not many standard functions that satisfy the conditions enunciated earlier.

A. Hyperbolic Tangent

Here we admit that g is a hyperbolic tangent

$$g(\rho) = \tanh(E\rho). \tag{13}$$

In the above, the E parameter is an arbitrary positive number. Inserting the above equation into (12) and using the table of integrals [20, pp. 508], we obtain that

$$\begin{aligned}\tilde{f}_2(\mathbf{k}') = \frac{1}{|\mathbf{k}'|^2 - \beta^2} - \frac{1}{|\mathbf{k}'|} \frac{\pi}{4E} \\ \times \sum_{\pm} \frac{1}{\sinh((|\mathbf{k}'| \pm \beta)\frac{\pi}{2E})} \end{aligned} \tag{14}$$

where $\sinh$ is the hyperbolic sine, and the sum with index "$\pm$" represents the sum of two terms: one with the "$+$" sign and the other with the "$-$" sign. If we let the E parameter approach zero, the Fourier transform of function f_2 becomes the Fourier transform of $\Phi_{0,\pm}$. Hence, from (14), we find that

$$\tilde{\Phi}_{0,\pm}(\mathbf{k}') = \frac{1}{|\mathbf{k}'|^2 - \beta^2}. \tag{15}$$

Since from (8) we have that $\tilde{\Phi}_{0,\pm}(\mathbf{k}') = \tilde{f}_1(\mathbf{k}') + \tilde{f}_2(\mathbf{k}')$, we conclude that

$$\tilde{f}_1(\mathbf{k}') = \frac{1}{|\mathbf{k}'|} \frac{\pi}{4E} \sum_{\pm} \frac{1}{\sinh\left((|\mathbf{k}'| \pm \beta)\frac{\pi}{2E}\right)}. \tag{16}$$

Equations (13) and (16) together with (9) define the "hyperbolic tangent mixed domain representation" of the lattice Green function.

The mixed-domain representation is the sum of $\Phi_{p,1}$ and $\Phi_{p,2}$. Both of these terms are triple sums that, provided E is positive, converge exponentially. In the particular case $E = 0$, $\Phi_{p,1}$ vanishes and $\Phi_{p,2}$ reduces to the spatial representation (7). On the other hand, if E is infinite, $\Phi_{p,1}$ reduces to the spectral representation (5a) and $\Phi_{p,2}$ vanishes.

In general a small value of E favors the convergence of $\Phi_{p,1}$, whereas a large value of E favors the convergence of $\Phi_{p,2}$. The optimum value is the one that ensures that both series have approximately the same convergence rate. It can be verified that an appropriate choice for E is

$$E = \frac{1}{V_{\text{cell}}^{1/3}} \frac{\pi}{\sqrt{2}}. \tag{17}$$

With this choice, the mixed-domain representation typically converges very fast, and only a few terms need to be summed to calculate the Green function to machine precision.

B. Error Function

Here we admit that g is the error function

$$g(\rho) = erf(E\rho) \tag{18}$$

where the E parameter is an arbitrary positive number. The Fourier transform of f_2 is now given by

$$\tilde{f}_2(\mathbf{k}') = \frac{1}{|\mathbf{k}'|^2 - \beta^2} - \frac{1}{2|\mathbf{k}'|} \times \sum_{\pm} \frac{e^{-(|\mathbf{k}'| \pm \beta)^2/4E^2}}{|\mathbf{k}'| \pm \beta}. \tag{19}$$

Proceeding as in the previous section, we obtain that

$$\tilde{f}_1(\mathbf{k}') = \frac{1}{2|\mathbf{k}'|} \sum_{\pm} \frac{e^{-(|\mathbf{k}'| \pm \beta)^2/4E^2}}{|\mathbf{k}'| \pm \beta}. \tag{20}$$

Equations (18) and (20) together with (9) define the "error function mixed domain representation" of the lattice Green function. This mixed representation has properties analogous to those of the mixed representation introduced in the previous section. An appropriate choice for the E parameter is now

$$E = \frac{\sqrt{\pi}}{V_{\text{cell}}^{1/3}}. \tag{21}$$

By direct inspection, one can verify that the convergence rate of this representation is significantly better than that of the hyperbolic tangent representation: it has Gaussian convergence rate.

IV. Representation of the Layer Green Function

Here we propose a new method to compute the layer Green function with exponential convergence rate. To begin with, we will prove that the lattice Green function and the layer Green function are intrinsically related.

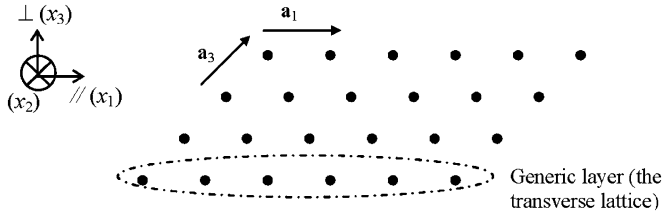

Fig. 1. The two-dimensional array of point sources defined by the primitive vectors $\mathbf{a}_1$ and $\mathbf{a}_2$, can be regarded as a sublattice of a three-dimensional array.

A. The Spectral-Like Representation

In what follows, we derive a representation of the lattice Green function analogous to the spectral representation (2) of the layer Green function. The idea is that the 3-D array of point sources can be regarded as the superimposition of 2-D arrays, as illustrated in Fig. 1. The building block of the lattice is a "layer" of point sources.

To exploit the referred property we rearrange the summation order in (4). We put

$$\Phi_p(\mathbf{u}) = \sum_{i_3} \left[\sum_{\bar{\mathbf{I}}} \Phi_0 \left(\mathbf{u} - \mathbf{r}_{\bar{\mathbf{I}}} - i_3 \mathbf{a}_3\right) e^{-j\mathbf{k}.\mathbf{r}_{\bar{\mathbf{I}}}} \right] e^{-ji_3 \mathbf{k}.\mathbf{a}_3}. \tag{22}$$

It is obvious that the term inside the rectangular brackets can be written in terms of the layer Green function. We have that

$$\Phi_p(\mathbf{u}) = \sum_n \Phi_H(\mathbf{u} - n\mathbf{a}_3) e^{-jn\mathbf{k}.\mathbf{a}_3} \tag{23}$$

where n is an arbitrary integer and Φ_H is the layer Green function associated with the transverse lattice defined by the primitive vectors $\mathbf{a}_1$ and $\mathbf{a}_2$. From the spectral representation of the layer Green function (2), we find that

$$\Phi_p(\mathbf{u}) = \sum_n \frac{1}{A_{\text{cell}}} \times \sum_{\bar{\mathbf{J}}} \frac{e^{-\gamma_{\mathbf{J}} |u_\perp - n a_{3\perp}|}}{2\gamma_{\bar{\mathbf{J}}}} e^{-j\mathbf{k}_{\bar{\mathbf{J}},//}.(\mathbf{u} - n\mathbf{a}_3)} e^{-jn\mathbf{k}.\mathbf{a}_3} \tag{24a}$$

$$\mathbf{k}_{\bar{\mathbf{J}},//} = \mathbf{k}_{//} + j_1 \mathbf{b}_{1//} + j_2 \mathbf{b}_{2//}$$

$$\gamma_{\bar{\mathbf{J}}} = \sqrt{|\mathbf{k}_{\bar{\mathbf{J}},//}|^2 - \beta^2}. \tag{24b}$$

We define $\mathbf{k}_{\bar{\mathbf{J}}}$ as

$$\mathbf{k}_{\bar{\mathbf{J}}} = \mathbf{k} + j_1 \mathbf{b}_1 + j_2 \mathbf{b}_2 \tag{25}$$

where $\mathbf{b}_1$ and $\mathbf{b}_2$ are the first two basis vectors of the reciprocal lattice. It is straightforward to verify that $\mathbf{b}_{1//}$ and $\mathbf{b}_{2//}$ (defined as in Section II) are the projections of $\mathbf{b}_1$ and $\mathbf{b}_2$ onto the transverse lattice plane. Hence $\mathbf{k}_{\bar{\mathbf{J}},//}$ is the projection of $\mathbf{k}_{\bar{\mathbf{J}}}$ onto the transverse plane.

Let $\hat{\mathbf{u}}_\perp$ be a unit vector normal to the transverse plane and $k_{\bar{\mathbf{J}},\perp}$ be the projection of $\mathbf{k}_{\bar{\mathbf{J}}}$ onto $\hat{\mathbf{u}}_\perp$. We have the decomposition $\mathbf{k}_{\bar{\mathbf{J}}} = \mathbf{k}_{\bar{\mathbf{J}},//} + \mathbf{k}_{\bar{\mathbf{J}},\perp} \hat{\mathbf{u}}_\perp$. Since $\mathbf{a}_3.\mathbf{b}_m = 0$ for $m = 1, 2$, we have that

$$(\mathbf{k} - \mathbf{k}_{\bar{\mathbf{J}},//}).\mathbf{a}_3 = \left(\mathbf{k} - \mathbf{k}_{\bar{\mathbf{J}}} + k_{\bar{\mathbf{J}},\perp} \hat{\mathbf{u}}_\perp\right).\mathbf{a}_3 = k_{\bar{\mathbf{J}},\perp} a_{3\perp}. \tag{26}$$

Thus, substituting (26) into (24) and interchanging the summation order, we obtain

$$\Phi_p(\mathbf{u}) = \frac{1}{A_{\text{cell}}} \sum_{\bar{\mathbf{J}}} \frac{e^{-j\mathbf{k}_{\bar{\mathbf{J}},//}.\mathbf{u}}}{2\gamma_{\bar{\mathbf{J}}}} \times \sum_n e^{-\gamma_{\mathbf{J}}|u_\perp - n a_{3\perp}|} e^{-jnk_{\mathbf{J},a_{3\perp}}}. \quad (27)$$

Next we assume that $|u_\perp| < |a_{3\perp}|$. In this case the series with index n in (27) consists of two geometrical series. These series are, respectively, the potentials from all the point sources above (below) the transverse lattice. Assuming, if necessary, that the wave number as a small negative imaginary component (which accounts for small losses and guarantees that the series converge), we readily obtain that

$$\Phi_p(\mathbf{u}) = \sum_{\bar{\mathbf{J}}} A_{\Phi,\bar{\mathbf{J}}}(u_\perp) e^{-j\mathbf{k}_{\mathbf{J},//}.\mathbf{u}} \quad (28a)$$

$$A_{\Phi,\bar{\mathbf{J}}}(u_\perp) = \frac{1}{A_{\text{cell}}} \frac{1}{2\gamma_{\bar{\mathbf{J}}}} \times \left(e^{-\gamma_{\mathbf{J}}|u_\perp|} + \sum_{\pm} \frac{e^{\pm\gamma_{\bar{\mathbf{J}}} u_\perp}}{e^{|a_{3\perp}|(\gamma_{\mathbf{J}} \pm j k_{\mathbf{J},\perp})} - 1} \right). \quad (28b)$$

In (28b) the sum with index "$\pm$" is a shorthand notation for the sum of two terms: one with "$+$" sign and the other with "$-$" sign.

Formula (28) is the "spectral-like" representation of the lattice Green function, relative to the transverse lattice defined by $\mathbf{a}_1$ and $\mathbf{a}_2$. It is valid only for $|u_\perp| < |a_{3\perp}|$. Nevertheless, we can always find a point $\mathbf{u}_0$ such that $|u_{0,\perp}| \leq |a_{3\perp}|/2$, and $\mathbf{u} = \mathbf{u}_0 + n\mathbf{a}_3$ for some n integer. Since the Green function is a Floquet wave with wave vector $\mathbf{k}$, we have that $\Phi_p(\mathbf{u}) = \Phi_p(\mathbf{u}_0)\exp(-j\mathbf{k}.\mathbf{a}_3 n)$, and thus we can use the spectral-like representation to evaluate the Green function in an arbitrary point of space.

We discuss next the convergence rate of the spectral-like representation. From the previous arguments it is clear that we can restrict our analysis to the case $|u_\perp| \leq |a_{3\perp}|/2$. We rewrite (28) as follows:

$$\Phi_p(\mathbf{u}) = \Phi_H(\mathbf{u}; \mathbf{a}_1, \mathbf{a}_2) + \Gamma_\Phi(\mathbf{u}; \mathbf{a}_1, \mathbf{a}_2, \mathbf{a}_3) \quad (29a)$$

$$\Gamma_\Phi(\mathbf{u}; \mathbf{a}_1, \mathbf{a}_2, \mathbf{a}_3) = \frac{1}{A_{\text{cell}}} \sum_{\bar{\mathbf{J}}} \frac{e^{-j\mathbf{k}_{\bar{\mathbf{J}},//}.\mathbf{u}}}{2\gamma_{\bar{\mathbf{J}}}} \times \sum_{\pm} \frac{e^{\pm\gamma_{\bar{\mathbf{J}}} u_\perp}}{e^{|a_{3\perp}|(\gamma_{\mathbf{J}} \pm j k_{\mathbf{J},\perp})} - 1}. \quad (29b)$$

In (29), we indicated explicitly in the argument of Φ_H that the transverse lattice is defined by $\mathbf{a}_1$ and $\mathbf{a}_2$. As we assume that $|u_\perp| \leq |a_{3\perp}|/2$, the auxiliary function Γ_Φ can be efficiently evaluated because the general term of the series decays exponentially. Therefore, it is clear from (29) that if one of the Green functions can be efficiently evaluated the other one also can. In Section IV–B, we use this property to accelerate the convergence of the layer Green function.

To conclude this section, and for the sake of completeness, we note that the convergence rate of the spectral-like representation of the lattice Green function is determined by the convergence rate of the layer Green function. Hence, the series (28) converges exponentially, except in the transverse plane $u_\perp = 0$ where it converges very slowly.

We also point out that the role of the primitive vectors $\mathbf{a}_1$, $\mathbf{a}_2$, and $\mathbf{a}_3$ in (28) can be interchanged by considering cyclic permutations of these vectors. Indeed, we can consider three distinct transverse lattices. Therefore we have at our disposal three alternative spectral-like representations for the lattice Green function. One of the representations is precisely (28). The other two representations are analogous to (28), but with one important difference: as the transverse lattice depends on the specific representation, so does the respective convergence rate. In fact, for each spectral-like representation, the region of slow convergence is the respective transverse lattice. In general, as much farther $\mathbf{u}$ is from a transverse lattice (we assume without loss of generality that $\mathbf{u}$ is in the unit cell), the better is the convergence of the associated spectral-like representation. However, if $\mathbf{u}$ is near the origin, the convergence rate is very poor for all representations. Thus the formulas derived in Section III are in general preferable.

B. The Acceleration Technique

Next, we explain how the layer Green function Φ_H can be computed using the results derived before.

We recall that Φ_H is the dynamic potential from a double-array of point sources at the lattice points $\mathbf{r}_{\bar{\mathbf{I}}} = i_1\mathbf{a}_1 + i_2\mathbf{a}_2$. The double-array is defined by the primitive vectors $\mathbf{a}_1$ and $\mathbf{a}_2$, and can be regarded as a sublattice of the array defined by the vectors $\mathbf{a}_1$, $\mathbf{a}_2$ and third arbitrary vector $\mathbf{a}_3$. The potential from the triple-array of point sources is the lattice Green function. From (29) we have the key result, which establishes that the layer Green function can be written in terms of the lattice Green function

$$\Phi_H(\mathbf{u}; \mathbf{a}_1, \mathbf{a}_2) = \Phi_p(\mathbf{u}) - \Gamma_\Phi(\mathbf{u}; \mathbf{a}_1, \mathbf{a}_2, \mathbf{a}_3) \quad \mathbf{u} = \mathbf{r} - \mathbf{r}'. \quad (30)$$

The formula is valid for $|u_\perp| < |a_{3\perp}|$. Note that (30) is valid for an arbitrary vector $\mathbf{a}_3$, and that the left-hand side is independent of $\mathbf{a}_3$.

The lattice Green function can be efficiently computed using one of the mixed-domain representations derived in Section III. On the other hand, the Γ_Φ function is a double series that converges fast provided $|u_\perp| \leq |a_3|/2$. Thus, the layer Green function can be efficiently computed using (30).

The vector $\mathbf{a}_3$ is chosen so that (30) converges as fast as possible. An adequate choice is

$$\mathbf{a}_3 = \sqrt{A_{\text{cell}}}\hat{\mathbf{u}}_\perp \quad (31)$$

where $\hat{\mathbf{u}}_\perp$ is a unit vector normal to the transverse lattice defined by $\mathbf{a}_1$ and $\mathbf{a}_2$. Since the layer Green function is independent of $k_\perp$, we can assume that the wave vector $\mathbf{k}$ is transverse. Thus, from (31), we have that $\mathbf{k}_{\bar{\mathbf{J}}} = \mathbf{k}_{\bar{\mathbf{J}},//}$, and (29b) simplifies to

$$\Gamma_\Phi(\mathbf{u}; \mathbf{a}_1, \mathbf{a}_2, \mathbf{a}_3) = \frac{1}{A_{\text{cell}}} \sum_{\bar{\mathbf{J}}} \frac{e^{-j\mathbf{k}_{\bar{\mathbf{J}},//}.\mathbf{u}}}{2\gamma_{\bar{\mathbf{J}}}} \frac{e^{\gamma_{\bar{\mathbf{J}}} u_\perp} + e^{-\gamma_{\bar{\mathbf{J}}} u_\perp}}{e^{\sqrt{A_{\text{cell}}}\gamma_{\bar{\mathbf{J}}}} - 1}. \quad (32)$$

Within the considered hypotheses, (30) is valid for $|u_\perp| < \sqrt{A_{\text{cell}}}$.

Thus, we propose the following strategy to compute the layer Green function in an arbitrary point $\mathbf{u}$. If $|u_\perp| > 0.5\sqrt{A_{\text{cell}}}$, the layer Green function can be efficiently computed using the spectral representation (2), and thus no acceleration technique is required. On the other hand, if $|u_\perp| < 0.5\sqrt{A_{\text{cell}}}$, the layer Green function is computed using (30), with $\mathbf{a}_3$ given by (31), and the lattice Green function calculated using a mixed-domain representation.

Usually the calculation of the layer Green function involves the computation of a double series [7], [9]. In contrast, the representation (30) involves the computation of Φ_p, and thus of a triple series. Apparently, this might suggest that the computational burden increases. In fact that is not the case, because the mixed-domain representation of lattice Green function converges extremely fast, and so the efficiency of the method is very good.

V. Numerical Simulations

A. The Convergence Rate of the Method

In this section, we compare the efficiency of the derived results with other formulas available from the open literature.

First we consider the mixed-domain formulas introduced in Section III for the lattice Green function. We compare our results with those yielded by Ewald's formula [13], which has Gaussian convergence rate. We implemented the numerical algorithms using the software application MATHEMATICA.[1]

As an example, we assume that the lattice is simple cubic with lattice constant a (i.e., the primitive vectors are orthogonal and such that $a \equiv |\mathbf{a}_1| = |\mathbf{a}_2| = |\mathbf{a}_3|$). The observation point is $\mathbf{r} = (0.1, 0, 0)a$, the wave vector is $\mathbf{k} = (0.5\pi/a, 0, 0)$, and the wave number is $\beta = 2\pi/(0.3a)$. We calculated the relative error in percentage, as a function of the computation time (normalized to arbitrary units). The result is depicted in Fig. 2. Note that the vertical axis is in logarithmic units. The reference value was obtained by summing the series with a very large number of terms.

As seen in Fig. 2, the error function representation is the most efficient, followed by the hyperbolic tangent representation. The least efficient method is that of Ewald's (curve c). Its computation time for the same numerical precision is about four times larger than that of the error function representation. It can be verified that theoretically the convergence rate of Ewald's formula is the same as that of the error function representation. The reason for the different computation times is related to the fact that Ewald's formula involves the calculation of the error function in the complex domain, which is computationally demanding. We also note that, in practice, a 0.1% error (-10 dB) in the Green function calculation is perfectly acceptable. In such conditions the efficiency of the hyperbolic function seems to be comparable to that of the error function.

The described conclusions are general and independent of the observation point and wave vector. Thus, we conclude that our mixed-domain representations are superior to Ewald's formula.

[1]MATHEMATICA 4.0, www.wolfram.com.

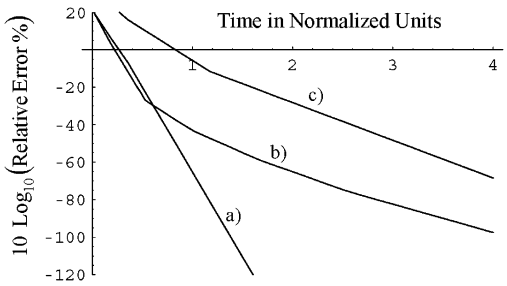

Fig. 2. Relative error in percentage (logarithmic scale) as a function of the computation time (normalized to arbitrary units). (a) Error function mixed-domain representation. (b) Hyperbolic tangent mixed-domain representation. (c) Ewald's formula. The wave number is $\beta = 2\pi/(0.3a)$.

TABLE I
Computation Error in Percentage as a Function of Parameter N_1

	Error Function Representation	Hyperbolic Function Representation
$N_1 = 1$	91.71%	91.87%
$N_1 = 2$	14.91%	14.63%
$N_1 = 3$	0.55%	0.71%
$N_1 = 4$	3.04×10^{-4}%	2.03×10^{-3}%
$N_1 = 5$	8.31×10^{-10}%	5.29×10^{-5}%
$N_1 = 6$	≈ 0	1.50×10^{-6}%

Besides that, they are much easier to implement computationally and thus they are of great relevance.

It is also appropriate to discuss the number of terms that we need to sum in order to calculate the Green function with good accuracy. Let us assume for simplicity that the summation range of the triple series in (9) is $|\mathbf{I}|, |\mathbf{J}| \leq N_1$, where $N_1 \geq 0$ is a nonnegative integer, $|\mathbf{I}| = \max\{|i_1|, |i_2|, |i_3|\}$, and $|\mathbf{J}|$ is defined similarly. Then, for a given N_1, the number of terms required to evaluate Φ_p is $2\times(2N_1 + 1)^3$. This value is not optimized and can be improved by imposing that only the terms of the series smaller than a given value are summed. For a computation error less than a few percent and a simple cubic lattice, it is in general sufficient to take $N_1 \approx 1 + \beta a/2\pi$.

In Table I, we present the relative error in percentage as a function of N_1. The lattice parameters are the same as before. As expected, the convergence rate of the error function representation is better asymptotically than that of the hyperbolic tangent representation. Nevertheless, for small N_1 the efficiency of the two representations is comparable. For fixed N_1, the accuracy gets better as the wave number β decreases. For example, for $\beta = 2\pi/(0.6a)$ and $N_1 = 2$, the error associated with the error function and hyperbolic function representations is only 0.051% and 0.39%, respectively.

In the rest of this section, we compare the convergence rate of (30) with Jordan *et al.*'s formula [9] for the layer Green function. We evaluated (30) always with the error function mixed-domain representation, because it has better convergence rate than the hyperbolic tangent representation.

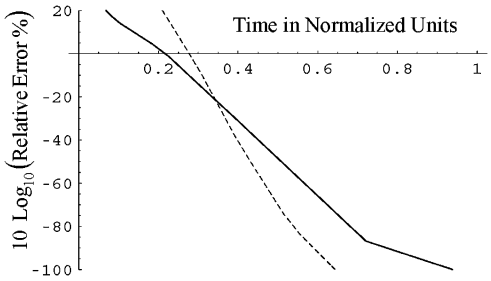

Fig. 3. Relative error in percentage (logarithmic scale) as a function of the computation time (normalized to arbitrary units). Full line: our results. Dashed line: Jordan *et al.*'s formula. The wave number is $\beta = 2\pi/(0.3a)$.

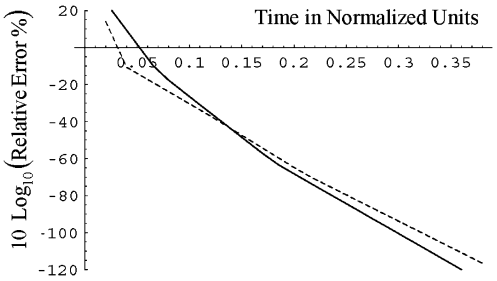

Fig. 4. Relative error in percentage (logarithmic scale) as a function of the computation time (normalized to arbitrary units). Full line: our results. Dashed line: Jordan *et al.*'s formula. The wave number is $\beta = 2\pi/(0.6a)$.

Jordan's formula is the generalization of Ewald's formula to double arrays of point sources in the three-dimensional space. Jordan's formula is a double series with Gaussian convergence rate and involves the computation of the error function in the complex plane. As discussed before, this aspect decisively worsens its global efficiency.

In the first example, we admit that the point sources are arranged into a square lattice with lattice constant a. The observation point and the wave vector are as before. The wave number is $\beta = 2\pi/(0.3a)$. In Fig. 3, we depict the relative error in percentage as a function of the computation time for representation (30) and Jordan's formula.

We see that the convergence rate of Jordan's formula is slightly better than that of (30), especially for a very high accuracy. The reason is mainly connected to the fact that representation (30) is a triple-series, whereas Jordan's formula is a double-series. But again, we note that in practical applications a 0.1% error $(-10\ \mathrm{dB})$ is perfectly acceptable.

In the second example, we consider that $\beta = 2\pi(0.6a)$. In Fig. 4, we depict the relative error as a function of the computation time. Now the convergence rate of both methods is approximately the same.

The simulated results show that the efficiency of both representations is comparable. Since (30) is easier to implement numerically, and since in most applications the required accuracy is moderate, we conclude that despite involving the calculation of a triple series, (30) is of great relevance and may help improving the performance of the existent electromagnetic solvers.

Next we discuss the number of terms that we need to sum in order to compute the layer Green function with good accuracy. We remind that from (30) the layer Green function is the sum of Φ_p with the auxiliary function Γ_Φ given by (32). We consider for simplicity that the summation range of the double series (32) is $|\bar{\mathbf{J}}| \leq N_2$, where $N_2 \geq 0$ is a nonnegative integer and $|\bar{\mathbf{J}}| = \max\{|j_1|, |j_2|\}$. Then, for a given N_2, the number of terms required to evaluate Γ_Φ is $(2N_2+1)^2$. For a computation error less than a few percent and a square lattice, an adequate value for N_2 is also $N_2 \approx 1 + \beta a/2\pi$. So, it is clear that most of the computational burden is related to the calculation of Φ_p, which was discussed before.

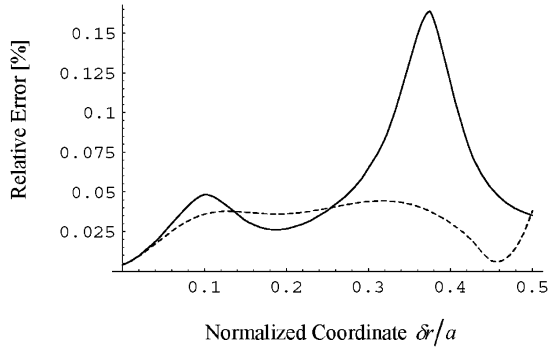

Fig. 5. Relative error as a function of the position of the observation point in the unit cell. Full line: scan on the source plane. Dashed line: scan on the direction normal to the source plane.

The convergence rate of the proposed method is practically independent of the position of the observation point in the unit cell. This is demonstrated in Fig. 5, where we plot the relative error in percentage as a function of the observation point coordinates. In the calculations we considered $N_1 = N_2 = 2$ (i.e., 275 terms were summed). We studied two cases: the full line results assume that $\mathbf{r} = (\delta r, 0.01a, 0)$ (scan on the source plane), whereas the dashed line results assume that $\mathbf{r} = (0, 0.01a, \delta r)$ (scan on the direction normal to the source plane), where $0 < \delta r/a < 0.5$. The wave number and the wave vector are as in the previous example. As seen in Fig. 5, the error is always less than 0.2% for every observation point. This clearly evidences the efficiency of the method.

B. Photonic Crystal Example

In this section, as an example of application of the derived Green functions, we characterize the dispersion characteristic of a three-dimensional array of square patches. The objective is to compute the electromagnetic modes of the periodic structure, more specifically the (normalized) resonant frequencies $\beta = \omega/c$ associated with a given wave vector $\mathbf{k}$. The unit cell of the periodic medium is depicted in Fig. 6. The square patch in the unit cell is denoted by ∂D. We assume that the host medium is air and that the square patches are perfect conductors. The periodic medium is obtained by translations of the unit cell along the primitive vectors.

In what follows, we briefly describe an integral equation based formulation to compute the electromagnetic modes. This formulation is conceptually equivalent to that described in [21].

Let $\mathbf{J}_c$ be the current density over ∂D. As is well known, the electromagnetic field radiated from the metallic obstacle can be derived from a vector potential with the free-space kernel Φ_0. The total electromagnetic field in the photonic crystal is the superimposition of the fields radiated by all the obstacles. Since the current density over a generic obstacle is $\mathbf{J}_c$ modulated by

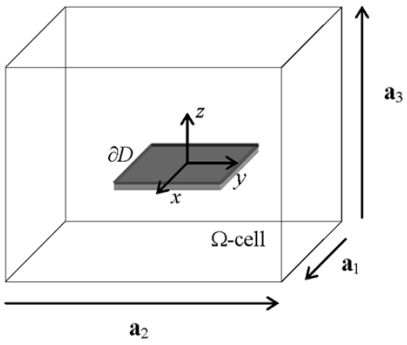

Fig. 6. Unit cell of a three-dimensional array of square patches.

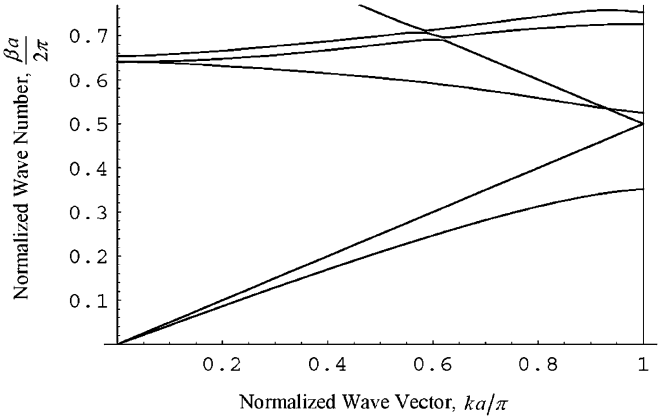

Fig. 7. Dispersion characteristic of the periodic medium (propagation along the x-axis).

the propagation factor $\exp(-j\mathbf{k}\cdot\mathbf{r})$, it is clear that the total field is

$$\mathbf{E}(\mathbf{r}) = \frac{Z_0}{j\beta}\nabla\times\nabla\times\int_{\partial D}\mathbf{J}_c(\mathbf{r}')\Phi_p(\mathbf{r}|\mathbf{r}';\beta,\mathbf{k})ds' \qquad (33)$$

where Z_0 is the impedance of the host medium and Φ_p is the lattice Green function. We note that the Green function depends on both β and $\mathbf{k}$.

Next, we obtain an integral equation for the current density. To this end, we impose that the tangential component of the electric field given by (33) vanishes over the metallic patch. We test (33) with a generic tangential density $\mathbf{w}$, and we integrate the resulting equation over ∂D. Using the standard method of moments procedure, we obtain that

$$\chi(\mathbf{w},\mathbf{J}_c)\equiv\int_{\partial D}\int_{\partial D}(\nabla_S\cdot\mathbf{w}^*(\mathbf{r})\nabla'_S\cdot\mathbf{J}_c(\mathbf{r}') - \beta^2\mathbf{w}^*(\mathbf{r})\cdot\mathbf{J}_c(\mathbf{r}'))\Phi_p(\mathbf{r}|\mathbf{r}';\beta,\mathbf{k})ds'ds = 0. \qquad (34)$$

In the above, the symbol "$*$" stands for the conjugate of a complex number and ∇_S. for the surface divergence. The previous result shows that an electromagnetic mode associated with the wave number β and the wave vector $\mathbf{k}$ is such that the corresponding current density $\mathbf{J}_c$ verifies (34) for an arbitrary test density $\mathbf{w}$.

We can use the above result to compute the dispersion characteristic $\beta=\beta(\mathbf{k})$ of the medium. To this end, we expand the current density in a basis of expansion functions $\mathbf{w}_1,\mathbf{w}_2,\ldots,\mathbf{w}_n$

$$\mathbf{J}_c=\sum_n c_n\mathbf{w}_n \qquad (35)$$

where c_n are the unknown coefficients of the expansion. Substituting (35) into (34) and choosing the test functions equal to the expansion functions, we obtain a homogeneous linear system of the form $[\chi_{m,n}][c_n]=0$, where $\chi_{m,n}=\chi(\mathbf{w}_m,\mathbf{w}_n)$. Obviously, a nontrivial solution may exist only if the determinant of the matrix vanishes. We use this fact to compute the resonant frequencies of the periodic medium. More specifically, for a given $\mathbf{k}$, we compute the solutions β of the equation $\det([\chi_{m,n}(\beta;\mathbf{k})])=0$, where $\det()$ stands for the determinant of the matrix. The zeros of the equation are calculated using the standard bisection method.

The described procedure requires a lot of computational effort because in each iteration we need to assemble the matrix $[\chi_{m,n}(\beta;\mathbf{k})]$ for a different β. This requires evaluating the lattice Green function thousands of times. It is therefore of crucial importance to compute the Green function efficiently, because otherwise the global efficiency of the method will be very poor.

In Fig. 7, we depict the first few bands of the computed dispersion characteristic for propagation along the x-axis (see Fig. 6). We considered that the primitive vectors are oriented along the coordinate axes, and that $a\equiv|\mathbf{a}_1|=|\mathbf{a}_2|=|\mathbf{a}_3|$ (simple cubic lattice). The area of the square patch is $0.7a^2$. We discretized the current using 36 expansion functions. In the static limit, two electromagnetic modes propagate in the periodic medium. The wave associated with the first fundamental band is characterized by a polarization (i.e., average electric field) along the y-direction. This wave interacts strongly with the metallic patches, and so it enters in cutoff in the frequency range $0.35<\beta a/2\pi<0.52$. On the other hand, the polarization of the wave associated with second band is along the z-direction. This wave does not interact with the metallic patches: it is an undisturbed free-space plane wave. The described structure can be used as a polarization-selective filter.

VI. Conclusion

In this paper, we proposed a new acceleration technique for the efficient computation of periodic Green functions. Besides having an excellent convergence rate, the proposed method is perfectly general, valid for arbitrary lattices, and works equally well irrespective of the relative position of the observation point in the unit cell. The Green function derivatives can also be easily computed from the derived formulas. The proposed formulas can be easily implemented in existent electromagnetic solvers and do not require the evaluation of complicated or cumbersome special functions.

We derived a new approach with exponential convergence rate to evaluate the layer Green function. Numerical simulations demonstrated that the computation time of our method is comparable to that of Jordan's formula (which is the unique method reported in the literature that also has exponential convergence rate). However, Jordan's formula is much more difficult to implement computationally.

In addition, we derived new representations for the lattice Green function. The lattice Green function has important applications in the study of photonic crystals and homogeniza-

tion theory. We believe that our approach to compute the lattice Green function is more efficient than any other method reported before in the literature.

To conclude, we note that in the characterization of FSSs and photonic crystals using integral equation methods the ratio between the computation times of two implementations that use different schemes to evaluate the Green function is approximately the same as the ratio between the computation times of the involved Green function schemes.

REFERENCES

[1] T. K. E. Wu, Ed., *Frequency Selective Surface and Grid Array*. New York: Wiley, 1995.

[2] A. Peterson, S. Ray, and R. Mittra, *Computational Methods for Electromagnetics*. New York: IEEE Press, 1998.

[3] E. Cohen, "Critical distance for grating lobe series," *IEEE Trans. Antennas Propag.*, vol. 39, pp. 677–679, May 1991.

[4] S. Singh, W. F. Richards, J. R. Zinecker, and D. R. Wilton, "Accelerating the convergence of series representing the free space periodic Green's function," *IEEE Trans. Antennas Propag.*, vol. 38, pp. 1958–1962, Dec. 1990.

[5] S. Singh and R. Singh, "Efficient computation of the free-space periodic Green's function," *IEEE Trans. Microwave Theory Tech.*, vol. 39, pp. 1226–1229, Jul. 1991.

[6] J. R. Mosig and A. Melcón, "The summation by parts algorithm—A new efficient technique for the rapid calculation of certain series arising in shielded planar structures," *IEEE Trans. Microwave Theory Tech.*, vol. 50, pp. 215–218, Jan. 2002.

[7] R. Jorgenson and R. Mittra, "Efficient calculation of the free-space periodic Green's function," *IEEE Trans. Antennas Propag.*, vol. 38, pp. 633–642, May 1990.

[8] R. Lampe, P. Klock, and P. Mayes, "Integral transforms useful for the accelerated summation of periodic, free-space Green's functions," *IEEE Trans. Microwave Theory Tech.*, vol. MTT-33, pp. 734–736, Aug. 1985.

[9] K. Jordan, G. Richter, and P. Sheng, "An efficient numerical evaluation of the Green's function for the helmholtz operator on periodic structures," *J. Comp. Phys.*, vol. 63, pp. 222–235, 1986.

[10] A. W. Mathis and A. F. Peterson, "Efficient electromagnetic analysis of a doubly infinite array of rectangular apertures," *IEEE Trans. Microwave Theory Tech.*, vol. 46, pp. 46–54, Jan. 1998.

[11] T. F. Eibert, J. L. Volakis, D. R. Wilton, and D. R. Jackson, "Hybrid FE/BI modeling of 3-D doubly periodic structures utilizing triangular prismatic elements and an MPIE formulation accelerated by the Ewald transformation," *IEEE Trans. Antennas Propag.*, vol. 47, pp. 843–850, May 1999.

[12] J. Callaway, *Quantum Theory of Solid State*. New York: Academic, 1991, ch. 1.

[13] P. P. Ewald, *Die Berechnung Optischer and Elektrostatischer Gitterpotentiale, Ann. Der Physik*, 1921, vol. 64, pp. 253–287.

[14] M. Silveirinha and C. A. Fernandes, "Effective permittivity of metallic crystals: A periodic Green's function formulation," *Electromagnetics*, no. 8, pp. 647–663, 2003.

[15] ——, "Efficient calculation of the band structure of artificial materials with cylindrical metallic inclusions," *IEEE Trans. Microwave Theory Tech.*, vol. 51, pp. 1460–1466, May 2003.

[16] ——, "A hybrid method for the efficient calculation of the band structure of 3-D metallic crystals," *IEEE Trans. Microwave Theory Tech.*, vol. 52, pp. 889–902, Mar. 2004.

[17] J. Joannopoulos, R. Meade, and J. Winn, *Photonic Crystals*. Princeton, NJ: Princeton Univ. Press, 1995.

[18] N. A. Nicorovici, R. C. McPhedran, and B. Ke-Da, "Propagation of electromagnetic waves in periodic lattices of spheres: Green's function and lattice sums," *Phys. Rev. E* , vol. 51, pp. 690–702, 1995.

[19] J. S. Walker, *Fourier Analysis*: Oxford University Press, 1988.

[20] I. S. Gradshteyn and I. M. Ryzhik, *Table of Integrals, Series, and Products*, 6th ed. New York: Academic, 2000.

[21] J. L. Blanchard, E. H. Newman, and M. Peters, "Integral equation analysis of artificial media," *IEEE Trans. Antennas Propag.*, vol. 42, pp. 727–731, May 1994.

Mário G. Silveirinha (S'99–M'03) received the Licenciado degree in electrical engineering from the University of Coimbra, Portugal, in 1998 and the Ph.D. degree in electrical and computer engineering from Instituto Superior Técnico (IST), Technical University of Lisbon, Portugal, in 2003.

His research interests include propagation in photonic crystals and homogenization and modeling of metamaterials.

Carlos A. Fernandes (S'86–M'89) received the Licenciado, M.Sc., and Ph.D. degrees in electrical and computer engineering from Instituto Superior Técnico (IST), Technical University of Lisbon, Lisbon, Portugal, in 1980, 1985, and 1990, respectively.

He joined IST in 1980, where since 1993 he has been an Associate Professor in the Department of Electrical and Computer Engineering in the areas of microwaves, radiowave propagation, and antennas. Also since 1993 he has been a Senior Researcher at the Instituto de Telecomunicações, where he currently is the Coordinator of the Wireless Communications scientific area. He has been the Leader of the antenna activity in National and European Projects as RACE 2067—MBS and ACTS AC230—SAMBA. He has coauthored a book, a book chapter, and several technical papers in international journals and conference proceedings in the areas of antennas and radiowave propagation modeling. His current research interests include artificial dielectrics, dielectric antennas for millimeter-wave applications, and propagation modeling for mobile communication systems.